MESSENGER orbital observations of large-amplitude Kelvin-Helmholtz waves at Mercury's magnetopause

Torbjörn Sundberg[1], Scott A. Boardsen[1,2], James A. Slavin[3], Brian J. Anderson[4], Haje Korth[4], Thomas H. Zurbuchen[3], Jim M. Raines[3], and Sean C. Solomon[5]

[1] Heliophysics Science Division, NASA Goddard Space Flight Center, Greenbelt, MD 20771, USA; [2] Goddard Earth Sciences and Technology Center, University of Maryland, Baltimore County, MD 21228, USA; [3] Department of Atmospheric, Oceanic and Space Sciences, University of Michigan, Ann Arbor, MI 48109, USA; [4] The Johns Hopkins University Applied Physics Laboratory, Laurel, MD 20723, USA; [5] Department of Terrestrial Magnetism, Carnegie Institution of Washington, Washington, DC 20015, USA.

Abstract

We present a survey of Kelvin-Helmholtz (KH) waves at Mercury's magnetopause during MESSENGER's first Mercury year in orbit. The waves were identified on the basis of the well-established sawtooth wave signatures that are associated with non-linear KH vortices at the magnetopause. MESSENGER frequently observed such KH waves in the dayside region of the magnetosphere where the magnetosheath flow velocity is still sub-sonic, which implies that instability growth rates at Mercury's magnetopause are much larger than at Earth. We attribute these greater rates to the limited wave energy dissipation in Mercury's highly resistive regolith. The wave amplitude was often on the order of 100 nT or more, and the wave periods were ~10-20 s. A clear dawn-dusk asymmetry is present in the data, in that all of the observed wave events

occurred in the post-noon and dusk-side sectors of the magnetopause. This asymmetry is likely related to finite Larmor-radius effects and is in agreement with results from particle-in-cell simulations of the instability. The waves were observed almost exclusively during periods when the north-south component of the magnetosheath magnetic field was northward, a pattern similar to that for most terrestrial KH wave events. Accompanying plasma measurements show that the waves were associated with the transport of magnetosheath plasma into the magnetosphere.

1. Introduction

On 18 March 2011 the MErcury Surface, Space ENvironment, GEochemistry, and Ranging (MESSENGER) spacecraft performed a successful Mercury orbit insertion (MOI) and is now the first spacecraft to provide continuous *in situ* data from the innermost planet. Together with measurements from the Mariner 10 and MESSENGER flybys of the planet, the collected data have revealed a small, yet complex magnetospheric system [*Anderson et al.*, 2008; *Zurbuchen et al.*, 2008; *Slavin et al.*, 2008]. Although it bears resemblance to a scaled-down version of the terrestrial case, Mercury's magnetosphere exhibits several differences that fundamentally affect the system's behavior. Mercury's proximity to the Sun together with the planet's comparatively weak dipole moment create a very dynamic system, with a reconnection rate far greater than what is typically seen at Earth [*Slavin et al.*, 2009]. The comparatively strong interplanetary magnetic field (IMF) drives intense substorms with loading-unloading times as short as 2-3 minutes [*Slavin et al.*, 2010]. In contrast to the other terrestrial planets, Mercury does not possess a substantial collision-dominated atmosphere, but rather a very tenuous exosphere of planetary atoms and molecules. The high solar radiation at Mercury's orbit leads to rapid photo-ionization,

which creates an ionized extension of the exosphere (primarily Na^+) throughout the magnetosphere [*Zurbuchen et al.*, 2008, 2011; *Raines et al.*, 2011]. The presence of heavy ions is expected to influence the dynamics of many of the magnetospheric processes, introducing kinetic effects into the system as the ion Larmor radii become large compared with the scale of the magnetosphere. Additionally, there is no conducting ionosphere around the planet, which means that any field-aligned current (FAC) system must close through Mercury's resistive regolith. Possible FAC signatures were observed during the first Mariner 10 flyby [*Slavin et al.*, 1997], but no evidence supporting the existence of FAC systems has yet been reported from MESSENGER observations.

In this paper, we present a survey of the magnetospheric Kelvin-Helmholtz (KH) instability during MESSENGER's first Mercury year (88 days) in orbit. Kelvin-Helmholtz waves are known to develop at a planetary magnetopause, where small-scale perturbations gain energy from the velocity shear between the magnetospheric and magnetosheath plasma and thereby grow into large-scale rolled-up vortices. Eventually, as the waves reach a turbulent state, they lead to the transfer of both plasma and energy from the dense magnetosheath into the more rarified magnetosphere. There exists considerable observational evidence for KH waves on both the dawn and dusk flank of the terrestrial magnetosphere, spanning approximately from the dawn-dusk meridian to 30 Earth radii down the magnetotail [*e.g., Chen and Kivelson,* 1993; *Chen et al.*, 1993; *Kokubun et al.,* 1994; *Fairfield et al.*, 2000, 2003, 2007; *Otto and Fairfield,* 2000; *Farrugia et al.*, 2000; *Hasegawa et al.*, 2004]. All of these wave events were reported in vicinity of the equatorial plane, where the magnetopause is believed to be susceptible to the KH instability [*e.g., Hasegawa et al.*, 2004; *Foullon et al.*, 2008]. KH wave activity has also been

observed at both the inner and outer boundaries of Saturn's low-latitude boundary layer [*Masters et al.*, 2009, 2010; *Delamere et al.,* 2011] and at the ionopause of Venus [*Pope et al.*, 2010]. A majority of the KH observations that have been reported from Earth cover periods of northward IMF. Such a condition is believed most favorable for the development of the instability. The northward direction of the field minimizes the field line tension in the direction of the streaming, which otherwise can have an inhibiting effect on the instability [*Chandrasekhar*, 1961]. The northward component also prevents reconnection at the dayside magnetopause, which in turn makes the closed dayside surface directly accessible to the impinging solar wind plasma and thereby increases the size of the viscous interaction region [*Burch et al.*, 1985]. For southward IMF, flux transfer events generated by dayside reconnection may also disrupt the evolution of KH vortices [*Hwang et al.*, 2011].

A series of KH waves was observed during MESSENGER's third Mercury flyby (M3) on 29 September 2009 [*Boardsen et al.*, 2010] as the spacecraft crossed the equatorial dusk-side magnetosphere. During that event, observed large-scale features in the magnetic field data were similar to those during many terrestrial events, including both abrupt inbound/outbound crossings of the magnetopause (as determined by the magnetic field magnitude) and sawtooth oscillations in the equatorial components of the field. Unfortunately, no high-resolution plasma measurements were available for this event. By applying a minimum variance analysis to the attributed magnetopause crossings, *Boardsen et al.* [2010] determined the magnetopause orientation at each wave encounter and showed that the measurements could be interpreted as a train of highly steepened surface waves propagating past the spacecraft with a period of about 16 s and a wavelength of ~2800 km. In a further analysis of the event, *Sundberg et al.* [2011]

showed that by taking advantage of MESSENGER's rapid crossing of the magnetopause region, a quasi-steady rolled-up vortex structure could be reconstructed from the magnetic field measurements.

2. Coordinate System

With the extended coverage of Mercury's magnetic field available from the orbital phase of the MESSENGER mission, *Anderson et al.* [2011b] were able to specify the planetary dipole moment with high precision. They concluded that the magnetic field can be represented by a dipole of moment 195±10 nT R_M^3 (where R_M is Mercury's radius, 2440 km) centered 484±11 km north of the planet's equatorial plane. An upper limit on the dipole tilt angle of 3° relative to the planet's rotational axis was also determined.

In analogy with the geocentric solar magnetic (GSM) and geocentric solar ecliptic (GSE) coordinate systems frequently used for the terrestrial magnetosphere, a Mercury solar magnetospheric (MSM) coordinate system centered at the origin of the planetary dipole moment is now available. In MSM coordinates, the X-axis is directed outward from the magnetic dipole toward the Sun. The Y-axis is perpendicular to X and is positive in the direction opposite to the orbital motion of the planet. The Z-axis is in the direction of magnetic north (*i.e.*, normal to the planet's orbital plane and positive toward the north celestial pole), and completes the right-handed system. The MSM coordinate system thus corresponds to a northward shift of 484 km from Mercury solar orbital (MSO) coordinates.

3. Observations

In this study we primarily utilize data from the MESSENGER Magnetometer instrument [*Anderson et al.*, 2007] to identify and classify KH waves at the magnetopause. Following MOI, MESSENGER has been in an eccentric orbit around the planet, with an 82.5° inclination to the orbital plane, an apoapsis of ~7 R_M from the planet center, and a periapsis of ~1.1 R_M. The apoapsis, initially located at ~15:00 magnetic local time (MLT), progresses during the mission and makes a full revolution around Mercury's equatorial plane over the Mercury year. After an initial verification period, the Magnetometer instrument became fully operational on 22 March 2011. To avoid introducing any bias in the statistics connected to the spacecraft trajectory, we have limited our analysis to one complete Mercury year (88 Earth days), starting on 23 March and ending on 20 June 2011.

On the basis of terrestrial KH wave signatures, together with the KH wave observations during M3, we anticipate two dominant features in the wave patterns: sawtooth wave oscillations and/or periodic inbound and outbound magnetopause crossings. The sawtooth-like wave pattern, which is frequently observed in both the plasma and magnetic field data at Earth's magnetopause [*e.g.*, *Fairfield et al.*, 2007; *Hasegawa et al.*, 2009], has been interpreted as a gradual transition through a mixing region on the leading edge of a rolled-up KH vortex, followed by an abrupt transition at the stable trailing edge [*Fairfield et al.*, 2007]. Large-scale boundary oscillations due to a KH wave train in the linear stage of the instability are more difficult to separate from non-KH phenomena, such as boundary motions due to variations in solar wind pressure. In order to adequately determine the KH nature of these types of waves, a full minimum variance analysis of a series of consecutive boundary layer crossings is required [*e.g.*, *Fairfield et al.*, 2000].

During the 23 March – 20 June 2011 time period, we found evidence for six large-amplitude sawtooth-shaped wave trains, all of them in the post-noon and evening sectors of the magnetosphere. The spacecraft trajectory for each wave observation is given in Figure 1. The details of two examples are given in sections 3.1 and 3.2, and a statistical study of all six events is given in section 3.3.

3.1. Example 1 – 15 May 2011

On 15 May 2011, MESSENGER's periapsis was located on the post-noon side of the planet, inside the dayside magnetosphere, at approximately 14:50 MLT, as shown in Figure 2. An overview of the magnetic field measurements is given in Figure 3. The spacecraft approached the equatorial plane from the north. Soon after the spacecraft's closest approach (CA) to the planet at 09:11:50 UTC, the Magnetometer recorded an extended interval of strong oscillations in the magnetic field, **B**, with a periodicity of 30–40 s. The amplitude of the perturbations was at its strongest nearest CA, starting at 45° magnetic latitude, approximately 1 R_M from the dipole center, with a peak-to-peak value of ~20 nT, and then decreased smoothly as MESSENGER traveled toward the post-noon side of the magnetosphere. The oscillations died out for an interval of ~2 minutes in the middle of the dayside magnetosphere, ~09:20:30–09:22:30 UTC, although an approximate wave pattern could still be discerned in B_y and B_z during this period.

As the spacecraft approached the magnetopause, the oscillations reappeared, first as small-amplitude fluctuations in all components of the magnetic field, and soon thereafter as large-amplitude oscillations with variations up to nearly 40 nT peak to peak in the B_x component

together with a sawtooth-like wave pattern in B_y. All wave activity stopped about 1 min before the magnetopause crossing (encountered at ~09:31:20) at the same time that the plasma count rate increased toward magnetosheath values. No further wave activity was seen after that time. The magnetic field remained strongly northward throughout the magnetosheath and in the solar wind for more than an hour after the wave encounters.

A close-up view of the magnetic field signatures of the KH waves is shown in Figure 3, together with supporting plasma data from MESSENGER's Fast Imaging Plasma Spectrometer (FIPS) [*Andrews et al.*, 2007]. The pattern indicates that large, non-linear (plausibly rolled-up) plasma waves were present inside the dayside magnetopause, penetrating on the order of 0.25 R_M (~600 km) into the magnetosphere, or almost a third of the distance to the planetary surface. The spatial extent of the waves was thus similar to that for the KH event seen during the third flyby, but the full spatial structure is in this case difficult to determine as the spacecraft trajectory was not confined to the planet's equatorial plane. The plasma measurements also showed clear periodic signatures of magnetosheath plasma at each wave encounter. The repeated pattern of the particle observations inside the magnetopause indicates that magnetosheath plasma was already being merged into the magnetosphere by KH waves in the post-noon sector of the magnetopause. Although no magnetic field perturbations are visible on the magnetosheath side of the magnetopause, periodic variations in the proton count rate by up to a factor of 2 are present in the plasma data. There is also a periodic pattern in the density of sodium ions that is consistent with the magnetic field oscillations. Notable Na^+ count rates are visible throughout most of the boundary layer when the plasma and magnetic field are magnetospheric, but no clear signature of Na^+ is seen when the magnetosheath plasma is present. These observations imply that the

increased H^+ count rates are actual encounters with magnetosheath plasma, and not the signature of compressional waves propagating inwards from the KH-unstable boundary [*e.g.*, *Pu and Kivelson*, 1983a, b].

The absolute magnitude of the field showed a two-peak feature similar to that reported by *Sundberg et al.* [2011] and was particularly visible during the time period 09:26–09:28. This pattern is indicative of the increase in the magnetic pressure at the edge of a vortex that is required to balance the centrifugal force acting on the plasma [*Miura*, 1997; *Hasegawa et al.*, 2009; *Nishino et al.*, 2011] and can be interpreted as a sign of the rolled-up nature of the waves.

A closer analysis of the wave pattern in the low-altitude region (09:14:00–09:17:40) shows an extremely stable wave pattern, primarily transverse albeit with a compressional component. The pulsations in minimum variance coordinates [*Sonnerup and Schieble*, 1998] and the associated magnetic hodogram are given in Figures 4 and 5, respectively. We have here applied a quadratic detrending of the data in order to remove the influence of the overall changes in the magnetic field magnitude and direction over the time period analyzed. The waves were elliptically polarized with an ellipticity of 0.6, and the approximate directions of maximum, intermediate, and minimum variance in MSM coordinates were (-0.9, 0.3, 0), (0.3, 0.8, 0.5), and (-0.2, -0.5, 0.9), respectively. The direction of minimum variance was clearly defined, with a ratio between the minimum- and intermediate-variance eigenvalues of 9.2, and the ratio of maximum to intermediate eigenvalue was 2.5. As the spacecraft MLT was steady at ~15:00 throughout the observations, and the pulsation frequency was relatively constant, it is a reasonable assumption that the high- and low-latitude wave oscillations are on near-conjugate field lines. The low-

altitude oscillation would thus be the signature of field-aligned waves propagating downward from the KH-instability region toward the planetary surface.

3.1. Example 2 – 17 June 2011

Another KH event was recorded on 17 June 2011. As shown in Figure 1, MESSENGER was in an inbound trajectory on the dusk side at around 17:00 MLT and crossed the magnetopause at ~00:50 UTC, 1 R_M north of the orbital plane. The magnetic field measurements for this event are given in Figure 6. The magnetopause transition is characterized by a change in the magnetic field properties from the high-frequency fluctuations typical of the magnetosheath to the smoother magnetospheric field components [*e.g.*, *Sundberg et al.*, 2011]. There is also an increase in the average X-component of the field, but otherwise the field properties were continuous across the boundary.

In contrast to the 15 May event, the main wave activity is seen on the magnetosheath side of the magnetopause (as determined from the overall magnetic field properties), where sawtooth oscillations with amplitudes close to 150 nT show clear signs of a KH wavetrain propagating along the magnetopause boundary. Once inside the magnetosphere, the wave properties changed to a more sinusoidal character, with smoother variations in the field. In this event, the magnetospheric wave pattern is observable deep into the magnetosphere, on the order of 0.4 R_M from the magnetopause. The oscillations were visible until the spacecraft reached 57° magnetic latitude, approximately 1.13 R_M from the dipole center. Although the oscillation period was relatively stable, the waves did not show the same clear wave structure as the low-altitude pulsations on 15 May. This difference is possibly a result of variability in the solar wind

properties during the wave observations, as the 15 May observations showed an unusually stable northward-directed magnetic field in both the magnetosheath and the solar wind. Periodic variations in the H^+ density are also visible during this wave event, but they are not as clearly correlated with the magnetic field as during the 15 May event because the wave and sampling frequencies are similar in magnitude. An increase in the proton flux is seen in the low-altitude portion of the wave pattern (~00:55 – 00:59 UTC). This increase may be the signature of magnetosheath ions that have been introduced into the magnetosphere at the magnetopause through the KH waves and then consequently guided by the magnetospheric field toward lower latitudes. Verification of this inference requires a thorough analysis of the plasma data, however, and is beyond the scope of the present study.

3.3. Event Selection and Statistics

Six large-amplitude KH wave trains were identified in the Magnetometer data over the selected time period. The events were identified on the basis of large-amplitude fluctuations (>50 nT) in the magnetic field showing that a continuous series of sawtooth waves are present at the magnetopause. A few events during which minor KH-wave structures were observed but the KH wave motion was not the main source of the measured magnetic field fluctuations are not included further here. MESSENGER also measured a few consecutive inbound/outbound magnetopause crossings. Although these may be related to the KH instability (as shown by *Fairfield et al.* [2000] and *Otto and Fairfield* [2000]), they require a long period of continuous observations for the KH structure to be adequately determined. As we cannot ascertain that this magnetopause motion is not due to compression and expansion of the magnetosphere driven by pressure fluctuations in the solar wind, we have chosen not to include such events in the analysis.

The details of the identified events are given in Table 1. Data from the third Mercury flyby are also included as a comparison. The spacecraft trajectory for each wave observation is shown in Figure 1.

Histograms of the measured wave periods are shown in Figure 7. All events show a relatively stable wave period in the approximate range 10–40 s, with a typical variation within ±10 s of their mean value (except for a few outliers in the data). The third Mercury flyby is not included here as the wave signature differs greatly from those for the other events; see *Boardsen et al.* [2010] and *Sundberg et al.* [2011] for details. All events apart from M3 were accompanied by a northward magnetic field in the magnetosheath and a relatively smooth transition in the magnetic field properties from the magnetosheath to the magnetosphere.

A majority of the events were observed during a time interval 8 days in length during which MESSENGER was crossing the dusk-side magnetopause in the 17:00-19:00 MLT section of the magnetosphere. The events that were farthest tailward were marked by sawtooth oscillations that appeared to be primarily located in the magnetosheath, but the magnetospheric field was less affected by the waves than for the dayside events.

4. Discussion

The observations presented here show clear evidence that KH waves are frequently present at Mercury's post-noon and dusk-side magnetopause and that they can give rise to plasma transfer on the dayside magnetosphere and cause global magnetic field oscillations as the field lines are distorted by the plasma wave motion. In contrast at Earth, to the best of our knowledge, there

are no fully reliable KH observations on the dayside of the terrestrial magnetosphere. Only a few wave observations possibly linked to the KH instability have previously been reported from this region [*Aubry et al.*, 1971; *Kawano et al.*, 1994], but these may well have been the signature of a series of pressure pulses or flux transfer events propagating over the dayside rather than fully grown KH waves. The magnetic field oscillations observed here are larger in amplitude, 70-150 nT, than the typical 30–50 nT oscillations reported at Earth [*e.g.*, *Chen et al.*, 1993; *Foullon et al.*, 2008; *Fairfield et al.*, 2007], although the wave amplitude relative to the total local field is of the same order of magnitude. The wave period is also much shorter, ~10–20 s compared with ~3-5 min at Earth. It is thus evident that the KH growth rates are substantially higher at Mercury's magnetopause than at Earth. In addition, given the high pressures exerted by the sodium ion group over the dayside magnetosphere (in some regions dominant over that of H^+ [*Raines et al.*, 2011; *Zurbuchen et al.*, 2011]) and the clear presence of Na^+ ions during the 15 May event, we expect a strong effect of the heavy ions on the instability.

4.1. Kelvin-Helmholtz Contributions to the Low-latitude Boundary Layer

One of the discoveries reported by MESSENGER is the identification of a boundary layer in the equatorial dayside associated with a reduced magnetic field pressure, but with no marked change in the magnetic field direction [*e.g.*, *Anderson et al.*, 2008; *Slavin et al.*, 2008, 2009]. *Anderson et al.* [2011a] showed that this boundary layer is associated with enhanced fluxes of H^+ ions. This region, which by analogy to Earth has been termed the low-latitude boundary layer (LLBL), was observed during both the first and second Mercury flybys (M1 and M2), despite the different IMF conditions for the two encounters. The M1 observations showed a northward IMF and a relatively quiet magnetosphere, whereas the magnetosphere was strongly driven by southward

IMF during M2, with a high rate of magnetic reconnection ongoing at the dayside magnetopause. *Raines et al.* [2011] derived LLBL H^+ densities and temperatures from the FIPS measurements and reported that the measured H^+ thermal pressure was not sufficient to account fully for the pressure balance at the inner boundary of the layer, falling short by up to 1.6 nPa and 0.6 nPa during M1 and M2, respectively. For M1, this figure corresponds to three times the estimated proton pressure in the layer. The LLBL must therefore contain an additional plasma population not within the instrument's field of view. Suggested explanations include heavy pick-up ions from the exosphere that have been accelerated by the magnetosheath flow [e.g., *Slavin et al.*, 2008; *Sarantos et al.*, 2009] and solar wind protons that entered through the cusp and experienced gradient and curvature drift into the closed field line region of the LLBL [*Anderson et al.*, 2011a].

Until now, the Kelvin-Helmholtz instability has not been considered as a likely source for the LLBL plasma, as the instability was expected to be active only at the flanks of the magnetotail rather than along the dayside regions of the magnetopause. However, as the present set of observations show that the KH instability can be responsible for the transfer of magnetosheath plasma into the magnetosphere even within the dayside section of the magnetosphere, the instability therefore becomes a potential source of the LLBL plasma. The estimated surface penetration of the KH waves is somewhat lower than the LLBL thickness reported by *Anderson et al.* [2011a] (~1000–1100 km and ~1000–1400 during M1 and M2, respectively, or 0.4-0.6 R_M), but they are of the same order of magnitude. It should be noted that the LLBL measurements were taken near the equatorial plane on the dawn side of the planet, whereas the measurements here are made off the equatorial plane on the dusk side of the planet. It is still possible that KH

waves are frequently present in the equatorial region on the dawn side of the magnetosphere, although such waves can be expected to be less marked than those on the dusk side.

4.2. Dawn-dusk Asymmetry and Finite Larmor-radius Effects

The exclusive observation of KH waves at the post-noon and dusk-side flank of the magnetopause gives strong evidence of a dawn-dusk asymmetry in the instability growth rate, although we cannot ascertain that all KH unstable regions have been probed. The Z value of MESSENGER's magnetopause crossings varied with MLT, and in general the spacecraft crossed the magnetopause off the magnetic equatorial plane, where we expect the main wave activity to occur. However, the data do give nearly symmetric coverage of dawn and dusk crossings (and in equal number), which helps to establish the asymmetry in the growth rates. Nonetheless, effects related to IMF direction during the time period of the observations cannot be fully ruled out.

Both analytical estimates [*e.g.*, *Nagano*, 1979; *Sanghvi and Chhajlani*, 1994] and simulations [*Huba, 1996*; *Nakamura et al.*, 2010] predict that finite Larmor-radius effects should affect the instability, and that the difference in the orientation of the velocity shear versus the vorticity on the dawn and dusk flanks should lead to asymmetries in the growth rates [*e.g.*, *Sundberg et al.*, 2010]. By the use of particle-in-cell simulations, *Nakamura et al.* [2010] quantified the effects of the ion gyrations and showed that the introduction of finite gyro radii in the KH simulations gave rise to an increased width of the velocity shear layer, which in turn reduced the growth rate of the instability. The difference in the direction of the velocity shear on the dawn and the dusk flanks leads to an increase in the ion gyro radii on the dawn-side magnetopause and a decrease on the dusk side. This difference was shown to have a noticeable effect on the growth rates on

the two sides, with the dusk-side magnetopause being much more unstable than the dawn side. These differences should be visible in both the linear and non-linear evolution of KH waves at Mercury's magnetopause. Contrary results were presented by *Delamere et al.* [2011]. With a hybrid simulation code, they investigated the effect of water group ions on the KH instability at Saturn and showed that the inclusion of heavy ions had only minor influence on wave growth. As the observations here are of wave activity solely on the dusk side, they are in agreement with the *Nakamura et al.* [2010] results. It is worth noting that this effect leads to reduced growth rates on both flanks compared with the magnetohydrodynamic wave solutions, and the simulations can therefore explain only the dawn-dusk asymmetry in the measurements and not the high growth rates in the post-noon sector of the magnetopause.

The analytical solutions show a somewhat different picture. Here, the finite Larmor radii are found to have a stabilizing or de-stabilizing effect for wavelengths near that of the maximum growth rate, dependent on the orientation of the velocity shear. *Nagano* [1979] showed that this effect leads to an increased maximum growth rate on the dawn side and a reduction in the growth rate on the dusk side at both Earth and Mercury. *Sanghvi and Chhajlani* [1994] and *Sundberg et al.* [2010] also reached the same conclusions, whereas *Glassmeier and Espley* [2006] reported the opposite effect. Although these results in principle predict an increase in the growth rate, they are generally contrary to the results presented here and therefore do not adequately explain the observed dusk-side growth rates.

4.3. Growth-rate Dependence on Solar Wind Properties

Mercury's proximity to the Sun leads to very different solar wind conditions at Mercury's orbit

than at Earth. By the solar wind scaling given by *Slavin and Holzer* [1981], the solar wind number density varies as r^{-2}, where r is the distance from the Sun in AU, and the magnetic field magnitude as $r^{-1}(r^{-2}+1)^{1/2}$. This scaling also leads to generally a lower value for plasma beta, the ratio of the plasma pressure to magnetic pressure, in the innermost solar system. As the instability is driven by the plasma motion and inhibited by the magnetic field tension, this scaling should give less favorable solar wind properties for the Kelvin-Helmholtz instability at Mercury's orbit. Additionally, due to the Parker spiral effect, the relative magnetic field increase is primarily in the radial component of the field, which leads to an additional depression of the instability [*Chandrasekhar*, 1961]. The effects of the sonic and Alfvén Mach numbers (M_A and M_S) on the growth rate were investigated by *Miura and Pritchett* [1982] and *Miura* [1992]. They found that both parameters had an effect on the instability, and the highest growth rates were for low M_S and high M_A. For the wave mode with propagation transverse to the magnetic field, shear flows below a critical Alfvén Mach number ~2 were found to be stable. The sonic Mach number has an opposite effect, with higher growth rates for low M_S. According to linear theory, flow shears with $M_S \geq 2$ should in principle be stable [*e.g.*, *Miura and Pritchett,* 1982], but simulations by *Miura* [1990] and *Kobayashi et al.*, [2008] have shown that KH waves can develop no matter how large the sonic Mach number. Although the Mach numbers in the solar wind should be slightly lower at Mercury's orbit, the magnetosheath profile should follow a behavior similar to that given by *Spreiter et al.* [1966], and the relative effect on the KH growth rates should be limited. We therefore find no reason to believe that the high growth rates implied by the observations reported here are directly related to the solar wind properties at Mercury's orbit.

4.4. Growth-rate Dependence on Planetary Conductivity

In a simulation performed by *Miura and Kan* [1992], it was shown that the ionospheric conductance has an important limiting effect on the KH instability. The line-tying effect of the ionosphere stabilizes the wave motion of the field line and provides energy dissipation in the form of ionospheric joule heating. Similar results were presented by *Keskinen et al.* [1988]. *Miura* [1996] also reported that an infinite ionospheric conductivity, which prevents any field-line slipping, would completely stabilize the field lines and prevent KH waves from developing at the magnetopause. These results can be applied to the MESSENGER observations. The large-amplitude oscillations observed near the planetary surface during the 15 May event show that energy dissipation in the exosphere and regolith is low. This inference is also supported by the lack of evidence for field-aligned currents in the low-altitude polar region of the planet. Mercury's lack of a conducting ionosphere and the low conductivity of the planet's regolith may well contribute to the high growth rates observed.

5. Summary

Although Mercury's magnetospheric dynamics are dominated by magnetic reconnection, we have shown that the KH instability plays a key role in driving the magnetosphere. Sawtooth oscillations of the magnetic field associated with the KH instability having a peak-to-peak amplitude of 100 nT or more are frequently present on the dusk side of Mercury's dayside magnetosphere. These waves involve plasma transfer into the magnetosphere, even in the dayside regions of the magnetosphere, and they are thus a potential source for the thick LLBL observed at the planet [*e.g.*, *Anderson et al.*, 2011a; *Raines et al.*, 2011]. The sawtooth oscillations are primarily present in the near-magnetosheath region, with lower-amplitude

oscillations visible far into the magnetosphere. One event, recorded on 15 May 2011, shows that the wave perturbations are present all along the affected field lines, down to the low-altitude foot point of the field.

A clear dawn-dusk asymmetry is seen in the data, with all the events recorded during MESSENGER's first Mercury year in orbit observed on the post-noon and dusk-side sections of the magnetosphere. These results are partly in agreement with those expected from finite Larmor-radius effects on the instability; simulations performed by *Nakamura et al.* [2010] have shown a clear dawn-dusk asymmetry in growth rates, with the dusk side being more prone to the instability. The greater growth rates at Mercury than at Earth cannot presently be explained by finite Larmor-radius effects. Although an abundance of heavy ions will affect the instability, heavy ions should primarily dampen the growth rates as they lead to a substantially broadened velocity shear region. The high growth rates are better explained, as predicted by the magnetohydrodynamic simulations of *Miura and Kan* [1992] and *Miura* [1996], by the lack of a conducting layer at the surface of the planet that can dissipate wave energy.

Acknowledgements

We thank two anonymous reviewers for constructive comments that improved the manuscript. The MESSENGER project is supported by the NASA Discovery Program under contracts NAS5-97271 to The Johns Hopkins University Applied Physics Laboratory and NASW-00002 to the Carnegie Institution of Washington. This research was also supported by an appointment to the NASA Postdoctoral Program at the Goddard Space Flight Center, administered by Oak Ridge

Associated Universities through a contract with NASA.

References

Anderson, B. J., M. H. Acuña, D. A. Lohr, J. Scheifele, A. Raval, H. Korth, and J. A. Slavin (2007), The Magnetometer instrument on MESSENGER, *Space Sci. Rev.*, *131*, 417–450.

Anderson, B. J., M. H. Acuña, H. Korth, M. E. Purucker, C. L. Johnson, J. A. Slavin, S. C. Solomon, and R. L. McNutt, Jr. (2008), The structure of Mercury's magnetic field from MESSENGER's first flyby, *Science*, *321*, 82–85.

Anderson, B. J., J. A. Slavin, H. Korth, S. A. Boardsen, T. H. Zurbuchen, J. M. Raines, G. Gloeckler, R. L. McNutt, Jr., and S. C. Solomon (2011a), The dayside magnetospheric boundary layer at Mercury, *Planet. Space Sci.*, *59*, 2037–2050.

Anderson, B. J., C. L. Johnson, H. Korth, M. E. Purucker, R. M. Winslow, J. A. Slavin, S. C. Solomon, R. L. McNutt, Jr., J. M. Raines, and T. H. Zurbuchen (2011b), The global magnetic field of Mercury from MESSENGER orbital observations, *Science*, *333*, 1859–1862.

Andrews, G. B., T. H. Zurbuchen, B. H. Mauk, H. Malcom, L. A. Fisk, G. Gloeckler, G. C. Ho, J. S. Kelley, P. L. Koehn, T. W. LeFevere, S. S. Livi, R. A. Lundgren, and J. M. Raines (2007), The Energetic Particle and Plasma Spectrometer instrument on the MESSENGER spacecraft, *Space Sci. Rev.*, *131*, 523–556.

Aubry, M. P., M. G. Kivelson, and C. T. Russell (1971), Motion and structure of the magnetopause, *J. Geophys. Res.*, *76*, 1673–1696.

Boardsen, S. A., T. Sundberg, J. A. Slavin, B. J. Anderson, H. Korth, S. C. Solomon, and L. G. Blomberg (2010), Observations of Kelvin-Helmholtz waves along the dusk-side boundary of Mercury's magnetosphere during MESSENGER's third flyby, *Geophys. Res. Lett.*, *37*, L12101, doi:10.1029/2010GL043606.

Burch, J. L., P. H. Reiff, J. D. Menietti, R. A. Heelis, W. B. Hanson, S. D. Shawhan, E. G. Shelley, M. Sugiura, D. R. Weimer, and J. D. Winningham (1985), IMF B_y-dependent plasma flow and Birkeland currents in the dayside magnetosphere, 1. Dynamics Explorer observations, *J. Geophys. Res.*, *90*, 1577–1593.

Chandrasekhar, S. (1961), *Hydrodynamic and Hydromagnetic Stability*, International Series of Monographs on Physics, Oxford Univ. Press, New York, 652 pp.

Chen, S.-H., and M. G. Kivelson (1993), On nonsinusoidal waves at the Earth's magnetopause, *Geophys. Res. Lett.*, *20*, 2699–2702.

Chen, S.-H., M. G. Kivelson, J. T. Gosling, R. J. Walker, and A. J. Lazarus (1993), Anomalous aspects of magnetosheath flow and of the shape and oscillations of the magnetopause during an interval of strongly northward interplanetary magnetic field, *J. Geophys. Res.*, *98*, 5727–5742, doi:10.1029/92JA02263.

Delamere, P. A., R. J. Wilson, and A. Masters (2011), Kelvin-Helmholtz instability at Saturn's magnetopause: Hybrid simulations, *J. Geophys. Res., 116*, A10222, doi:10.1029/2011JA016724.

Fairfield, D. H., A. Otto, T. Mukai, S. Kokubun, R. P. Lepping, J. T. Steinberg, A. J. Lazarus, and T. Yamamoto (2000), Geotail observations of the Kelvin-Helmholtz instability at the equatorial magnetotail boundary for parallel northward fields, *J. Geophys. Res.*, *105*, 21,159–21,173.

Fairfield, D. H., C. J. Farrugia, T. Mukai, T. Nagai, and A. Fedorov (2003), Motion of the dusk flank boundary layer caused by solar wind pressure changes and the Kelvin-Helmholtz instability: 10–11 January 1997, *J. Geophys. Res.*, *108*, 1460, doi:10.1029/2003JA010134.

Fairfield, D. H., M. M. Kuznetsova, T. Mukai, T. Nagai, T. I. Gombosi, and A. J. Ridley (2007), Waves on the dusk flank boundary layer during very northward interplanetary magnetic field conditions: Observations and simulation, *J. Geophys. Res.*, *112*, A08206, doi:10.1029/2006JA012052.

Farrugia, C. J., et al. (2000), Coordinated Wind, Interball/tail, and ground observations of Kelvin-Helmholtz waves at the near-tail, equatorial magnetopause at dusk: January 11, 1997, *J. Geophys. Res.*, *105*, 7639–7667.

Foullon, C., C. J. Farrugia, A. N. Fazakerley, C. J. Owen, F. T. Gratton, and R. B. Torbert (2008), Evolution of Kelvin-Helmholtz activity on the dusk flank magnetopause, *J. Geophys. Res.*, *113*, A11203, doi:10.1029/2008JA013175.

Fujimoto, M., W. Baumjohann, K. Kabin, R. Nakamura, J. A. Slavin, N. Terada, and L. Zelenyi (2007), Hermean magnetosphere–solar wind interaction, *Space Sci. Rev.*, *132*, 529–550, doi:10.1007/s11214-007-9245-8.

Glassmeier, K.-H., and J. Espley (2006), ULF waves in planetary magnetospheres, in *Magnetospheric ULF Waves: Synthesis and New Directions,* edited by K. Takahashi, P. J. Chi, R. E. Denton, and R. L. Lysak, Geophysical Monograph Ser., vol. 169, pp. 341–349, AGU, Washington, D. C.

Hasegawa, H., M. Fujimoto, T. Phan, H. Rème, A. Balogh, M.W. Dunlop, C. Hashimoto, and R. TanDokoro (2004), Transport of solar wind into Earth's magnetosphere through rolled-up Kelvin–Helmholtz vortices, *Nature*, *430*, 755–758.

Hasegawa, H., et al. (2009), Kelvin-Helmholtz waves at the Earth's magnetopause: Multiscale development and associated reconnection, *J. Geophys. Res.*, *114*, A12207, doi:10.1029/2009JA014042.

Huba, J. D. (1996), The Kelvin-Helmholtz instability: Finite Larmor radius magnetohydrodynamics, *Geophys. Res. Lett.*, *23*, 2907–2910, doi:10.1029/96GL02767.

Hwang, K.-J., M. M. Kuznetsova, F. Sahraoui, M. L. Goldstein, E. Lee, and G. K. Parks (2011), Kelvin-Helmholtz waves under southward interplanetary magnetic field, *J. Geophys. Res.*, *116*, A08210, doi:10.1029/2011JA016596.

Keskinen, M., H. Mitchell, J. Fedder, P. Satyanarayana, S. Zalesak, and J. Huba (1988), Nonlinear evolution of the Kelvin-Helmholtz instability in the high-latitude ionosphere, *J. Geophys. Res.*, *93*, 137–152.

Kawano, H., S. Kokubun, T. Yamamoto, K. Tsuruda, H. Hayakawa, M. Nakamura, T. Okada, A. Matsuoka, and A. Nishida (1994), Magnetopause characteristics during a four-hour interval of multiple crossings observed with GEOTAIL, *Geophys. Res. Lett.*, *21*, 2895–2898.

Kobayashi, Y., M. Kato, K. T. A. Nakamura, T. K. M. Nakamura, and M. Fujimoto (2008), The structure of Kelvin Helmholtz vortices with super-sonic flow, *Adv. Space Res.*, *41*, 1325–1330, doi:10.1016/j.asr.2007.04.016.

Kokubun, S., H. Kawano, M. Nakamura, T. Yamamoto, K. Tsuruda, H. Hayakawa, A. Matsuoka, and L. A. Frank (1994), Quasi-periodic oscillations of the magnetopause during northward sheath magnetic field, *Geophys. Res. Lett.*, *21*, 2883–2886.

Masters, A., N. Achilleos, C. Bertucci, M. K. Dougherty, S. J. Kanani, C. S. Arridge, H. J. McAndrews, and A. J. Coates (2009), Surface waves on Saturn's dawn flank magnetopause

driven by the Kelvin-Helmholtz instability, *Planet. Space Sci.*, 57, 1769–1778, doi:10.1016/j.pss.2009.02.010.

Masters, A., et al. (2010), Cassini observations of a Kelvin-Helmholtz vortex in Saturn's outer magnetosphere, *J. Geophys. Res.*, *115*, A07225, doi:10.1029/2010JA015351.

Miura, A. (1990), Kelvin-Helmholtz instability for supersonic shear flow at the magnetospheric boundary, *Geophys. Res. Lett.*, *17*, 749–752, doi:10.1029/GL017i006p00749.

Miura, A. (1992), Kelvin-Helmholtz instability at the magnetospheric boundary: Dependence on the magnetosheath sonic Mach number, *J. Geophys. Res.*, *97*, 10,655–10,675.

Miura, A. (1996), Stabilization of the Kelvin-Helmholtz instability by the transverse magnetic field in the magnetosphere-ionosphere coupling system, *Geophys. Res. Lett.*, *23*, 761–764.

Miura, A. (1997), Compressible magnetohydrodynamic Kelvin–Helmholtz instability with vortex pairing in the two-dimensional transverse configuration, *Phys. Plasmas*, *4*, 2871–2885, doi:10.1063/1.872419.

Miura, A., and J. R. Kan (1992), Line-tying effects on the Kelvin-Helmholtz instability, *Geophys. Res. Lett.*, *19*, 1611–1614.

Miura, A., and P. L. Pritchett (1982), Nonlocal stability analysis of the MHD Kelvin-Helmholtz instability in a compressible plasma, *J. Geophys. Res.*, *87*, 7431–7444.

Nagano, H. (1979), Effect of finite ion Larmor radius on the Kelvin–Helmholtz instability of the magnetopause, *Planet. Space Sci.*, *27*, 881–884.

Nakamura, T. K. M., H. Hasegawa, and I. Shinohara (2010), Kinetic effects on the Kelvin-Helmholtz instability in ion-to-MHD scale transverse velocity shear layers: Particle simulations, *Phys. Plasmas*, *17*, 042119, doi:10.1063/1.3385445

Nishino, M. N., H. Hasegawa, M. Fujimoto, Y. Saito, T. Mukai, I. Dandouras, H. Rème, A. Retinò, R. Nakamura, E. Lucek, and S. J. Schwartz (2011), A case study of Kelvin–Helmholtz vortices on both flanks of the Earth's magnetotail, *Planet. Space Sci.*, *59*, 502–509.

Otto, A., and D. H. Fairfield (2000), Kelvin-Helmholtz instability at the magnetotail boundary: MHD simulation and comparison with Geotail observations, *J. Geophys. Res.*, *105*, 21,175–21,190, doi:10.1029/1999JA000312.

Pope, S. A., M. A. Balikhin, T. L. Zhang, A. O. Fedorov, M. Gedalin, and S. Barabash (2009), Giant vortices lead to ion escape from Venus and re-distribution of plasma in the ionosphere, *Geophys. Res. Lett.*, *36*, L07202, doi:10.1029/2008GL036977.

Pu, Z.-Y., and M. G. Kivelson (1983a), Kelvin-Helmholtz instability at the magnetopause: Solution for compressible plasmas, *J. Geophys. Res.*, *88*, 841–852, doi:10.1029/JA088iA02p00841.

Pu, Z.-Y., and M. G. Kivelson (1983b), Kelvin-Helmholtz Instability at the magnetopause: Energy flux Into the magnetosphere, *J. Geophys. Res.*, *88*, 853–861, doi:10.1029/JA088iA02p00853.

Raines, J. M., J. A. Slavin, T. H. Zurbuchen, G. Gloeckler, B. J. Anderson, D. N. Baker, H. Korth, S. M. Krimigis, and R. L. McNutt, Jr. (2011), MESSENGER observations of the plasma environment near Mercury, *Planet. Space Sci.*, *59*, 2004–2015.

Sanghvi, R. K., and R. K. Chhajlani (1994), Hydromagnetic Kelvin–Helmholtz instability in the presence of suspended particles and finite Larmor radius effect, *Z. Naturforsch.*, *49a*, 1102–1110.

Sarantos, M., J. A. Slavin, M. Benna, S. A. Boardsen, R. M. Killen, D. Schriver, and P. Trávníček (2009), Sodium-ion pickup observed above the magnetopause during MESSENGER's first Mercury flyby: Constraints on neutral exospheric models, *Geophys. Res. Lett.*, *36*, L04106, doi:10.1029/2008GL036207.

Slavin, J. A., and R. E. Holzer (1981), Solar wind flow about the terrestrial planets, 1. Modeling bow shock position and shape, *J. Geophys. Res.*, *86*, 11,401–11,418.

Slavin, J. A., C. J. Owen, J. E. P. Connerney, and S. P. Christon (1997), Mariner 10 observations of field-aligned currents at Mercury, *Planet. Space Sci.*, *45*, 133–141.

Slavin, J. A., *et al.* (2008), Mercury's magnetosphere after MESSENGER's first flyby, *Science*, *321*, 85–89, doi:10.1126/science.1159040.

Slavin, J. A., *et al.* (2009), MESSENGER observations of magnetic reconnection in Mercury's magnetosphere, *Science*, *324*, 606–610.

Slavin, J. A., *et al.* (2010), MESSENGER observations of extreme loading and unloading of Mercury's magnetic tail, *Science*, *329*, 665–668.

Sonnerup, B. U. Ö., and M. Scheible (1998), Minimum and maximum variance analysis, in *Analysis Methods for Multi-Spacecraft Data,* edited by G. Paschmann and P. Daly, ISSI Scientific Reports Series, vol.1, pp.185–220, ESA/ISSI, Noordwijk, The Netherlands.

Spreiter, J. R., A. L. Summers and A. Y. Alksne (1966), Hydromagnetic flow around the magnetosphere, *Planet. Space Sci.*, *14*, 223–250.

Sundberg, T., S. A. Boardsen, J. A. Slavin, L. G. Blomberg, and H. Korth (2010), The Kelvin-Helmholtz instability at Mercury: An assessment, *Planet. Space Sci.*, *58*, 1434–1441, doi:10.1016/j.pss.2010.06.008.

Sundberg, T., S. A. Boardsen, J. A. Slavin, L. G. Blomberg, J. A. Cumnock, S. C. Solomon, B. J. Anderson, and H. Korth (2011), Reconstruction of propagating Kelvin-Helmholtz vortices at Mercury's magnetopause, *Planet. Space Sci.*, *59*, 2051–2057.

Zurbuchen, T. H., J. M. Raines, G. Gloeckler, S. M. Krimigis, J. A. Slavin, P. L. Koehn, R. M. Killen, A. L. Sprague, R. L. McNutt, Jr., and S. C. Solomon (2008), MESSENGER observations of the composition of Mercury's ionized exosphere and plasma environment, *Science, 321*, 90–92, doi:10.1126/science.1159314

Zurbuchen, T. H., J. M. Raines, J. A. Slavin, D. J. Gershman, J. A. Gilbert, G. Gloeckler, B. J. Anderson, D. N. Baker, H. Korth, S. M. Krimigis, M. Sarantos, D. Schriver, R. L. McNutt, Jr., and S. C. Solomon (2011), MESSENGER observations of the spatial distribution of planetary ions near Mercury, *Science, 333*, 1862–1865.

Table 1. Times and locations of KH waves observed at Mercury.

Date	DOY	Time interval	MLT, h	MSH B_z	Mean period	Maximum amplitude
29 Sep 2009	**272**	21:27 – 21:29	21	Variable	17 s[1]	40 nT
15 May 2011	**135**	09:13 – 09:30	15.5	North	36 s	100 nT
11 Jun 2011	**162**	12:36 – 12:37	19	North	12 s	135 nT
12 Jun 2011	**163**	00:28 – 00:36	19	North	20 s	70 nT
15 Jun 2011	**166**	13:10 – 13:20	18	North	15 s	120 nT
17 Jun 2011	**168**	00:45 – 00:58	17	North	17 s	150 nT
19 Jun 2011	**170**	23:33 – 23:43	16	North	24 s	75 nT

Notes: For each event, the time interval, approximate MLT, direction of the magnetosheath B_Z component, mean periodicity, and approximate maximum wave amplitude are given. DOY and MSH denote day of year and magnetosheath, respectively. [1]We here use the time estimate from *Boardsen et al.* [2010]. The wave interpretation given by *Sundberg et al.* [2011] specifies a stable wave period of 20 s.

Figure 1. Overview of MESSENGER's trajectory for the observed wave events. The trajectories in MSM coordinates for the full duration of the wave observations are shown by black lines, and the spacecraft position at the end of each event is given by a colored circle. The dashed lines show approximate locations of the magnetopause and the bow shock in the Z=0 (top left), X=0

(top right), and Y=0 (bottom left) planes. The bottom-right panel is given in the X-R plane, where $R = \sqrt{(Z^2 + Y^2)}$ is the radial distance from the X-axis. Data from MESSENGER's third Mercury flyby are included on all panels for comparison.

Figure 2. Overview of the KH wave observation on 15 May 2011. The panels show, from top to bottom, the X, Y, and Z components in MSM coordinates and the absolute magnitude of the magnetic field. The dashed line marks the approximate position of the magnetopause (MP) crossing.

Figure 3. A closer view of the KH waves of 15 May 2011. The top two panels show the FIPS spectrogram of energy E per charge Q for the measured proton flux and the sodium ion count rate, respectively. Panels 3-6 follow the same format as in Figure 2.

Figure 4. Close-up of the low-altitude pulsations. The figure shows, from top to bottom, the maximum (B_1), intermediate (B_2), and minimum (B_3) variance components and the absolute magnitude of the magnetic field after a quadratic detrending of the data. A 1-s smoothing filter has been applied to the data.

Figure 5. Hodogram of the magnetic field components in Figure 4.

Figure 6. KH observations on 17 June 2011, in the same format as in Figure 3.

Figure 7. Histograms of the observed wave periods for the six events observed during MESSENGER's first Mercury year in orbit. The median and mean values of the periods for each wave event are marked by dotted and dashed-dotted lines, respectively.

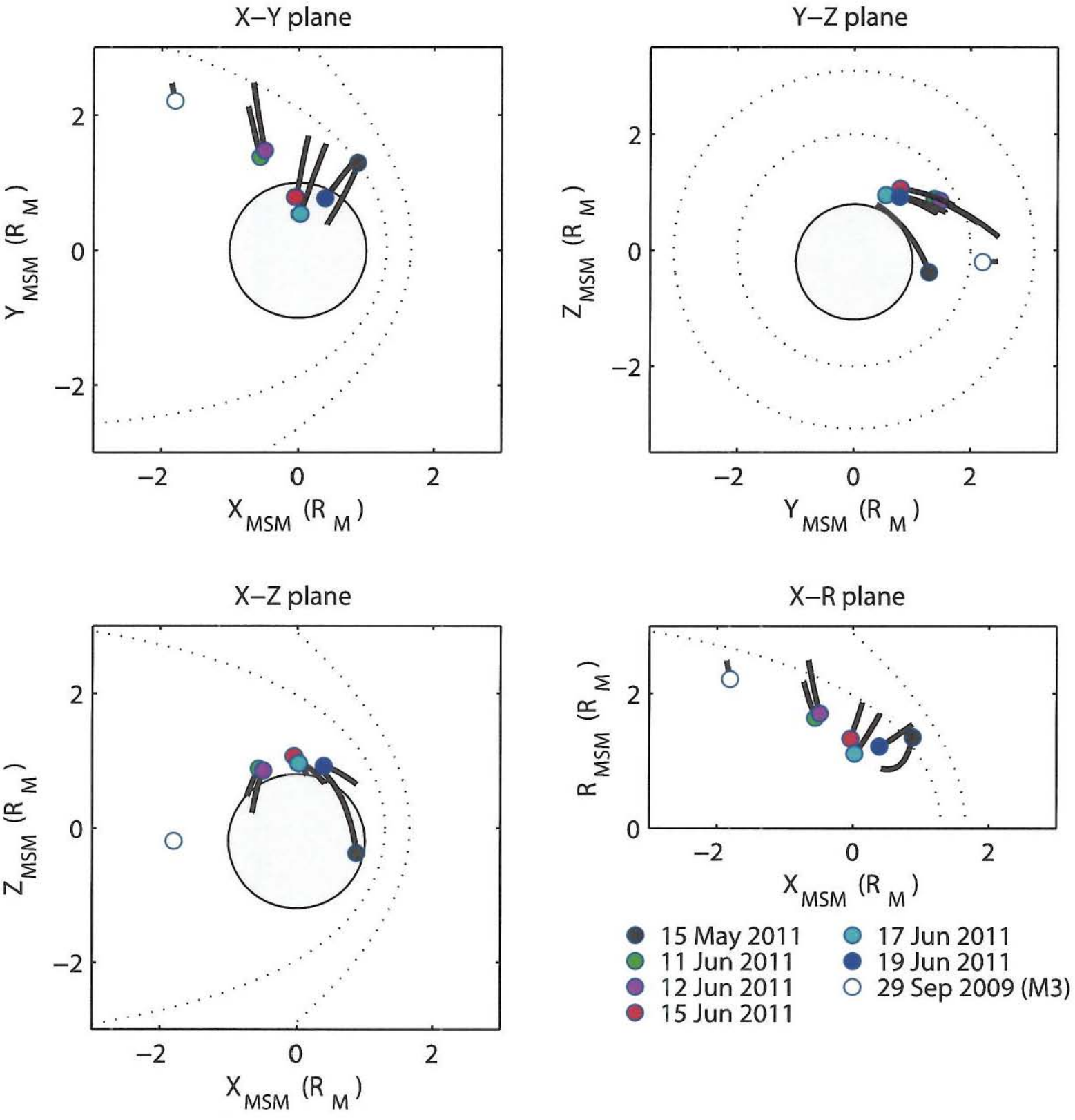
X–Y plane
Y–Z plane
X–Z plane
X–R plane
Y_{MSM} (R_M)
Z_{MSM} (R_M)
R_{MSM} (R_M)
X_{MSM} (R_M)
2
0
−2
15 May 2011
11 Jun 2011
12 Jun 2011
15 Jun 2011
17 Jun 2011
19 Jun 2011
29 Sep 2009 (M3)

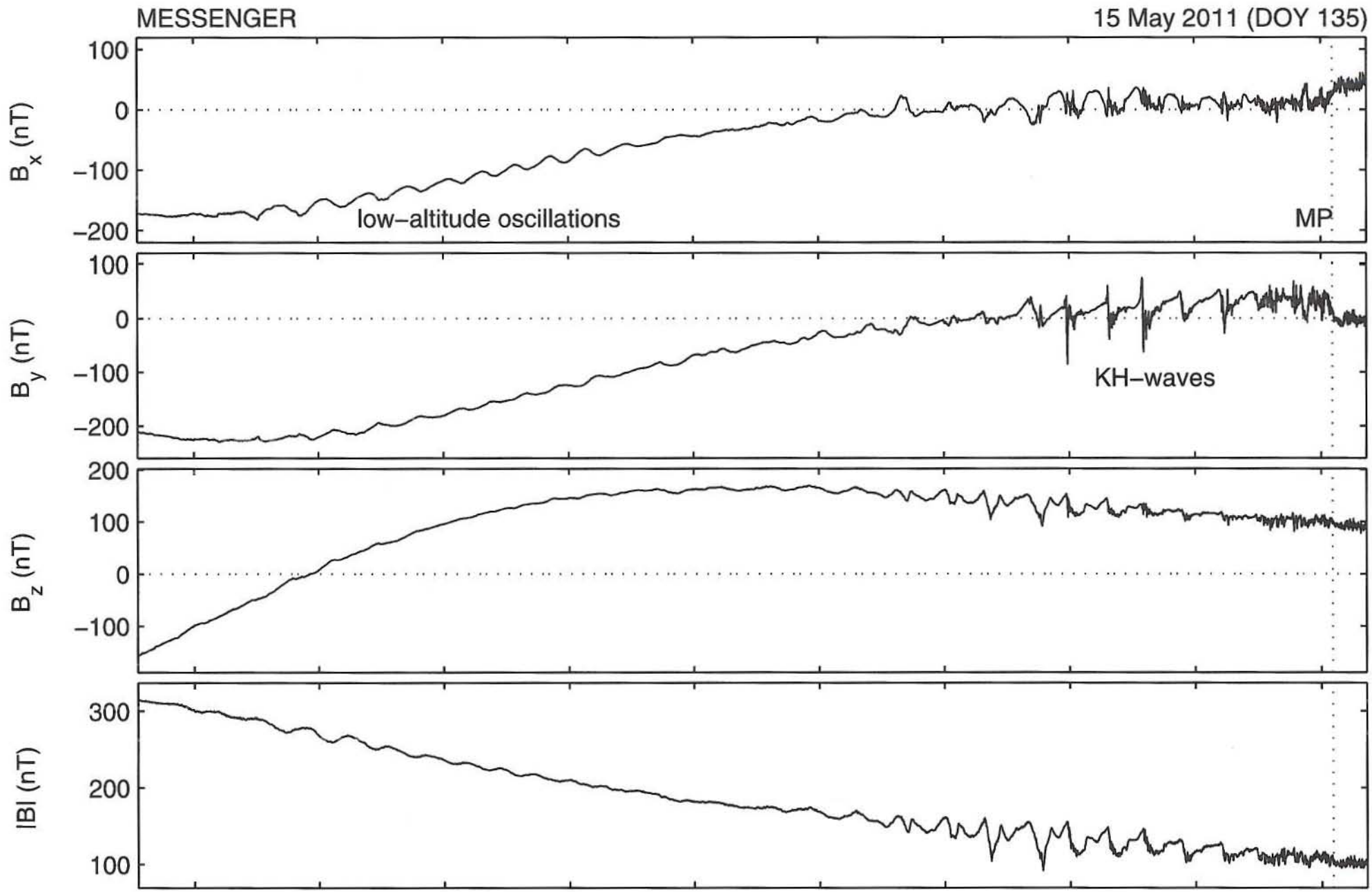

UTC	9:13:00	9:15:00	9:17:00	9:19:00	9:21:00	9:23:00	9:25:00	9:27:00	9:29:00	9:31:00
X_{MSM} (R_M)	0.45	0.53	0.6	0.66	0.71	0.76	0.8	0.83	0.86	0.88
Y_{MSM} (R_M)	0.44	0.57	0.7	0.81	0.91	1.01	1.09	1.17	1.23	1.29
Z_{MSM} (R_M)	0.76	0.66	0.55	0.43	0.3	0.17	0.03	−0.1	−0.24	−0.38

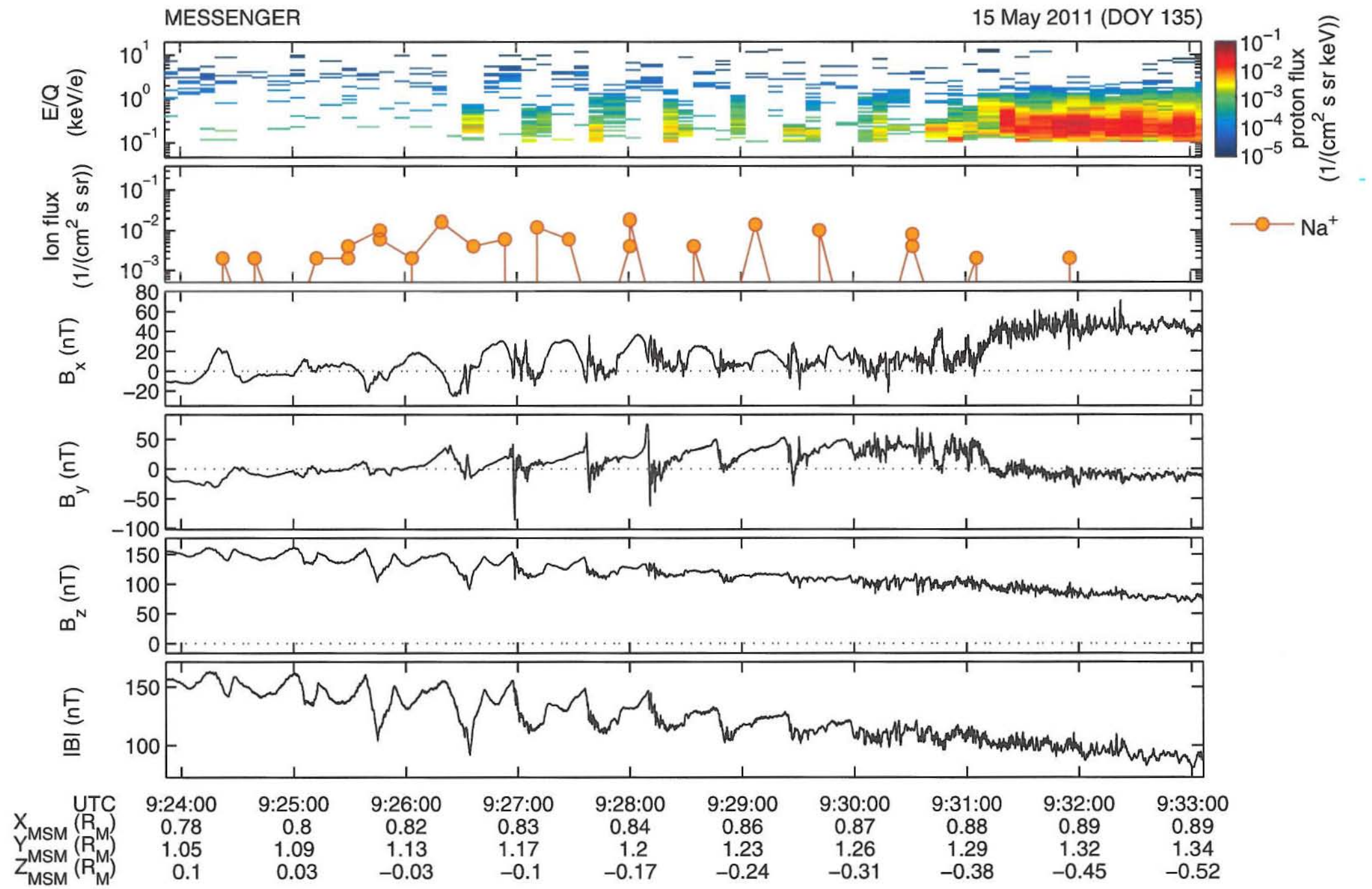
MESSENGER
15 May 2011 (DOY 135)
E/Q (keV/e)
proton flux (1/(cm² s sr keV))
Ion flux (1/(cm² s sr))
Na+
Bx (nT)
By (nT)
Bz (nT)
IBI (nT)
UTC 9:24:00 9:25:00 9:26:00 9:27:00 9:28:00 9:29:00 9:30:00 9:31:00 9:32:00 9:33:00
XMSM (RM) 0.78 0.8 0.82 0.83 0.84 0.86 0.87 0.88 0.89 0.89
YMSM (RM) 1.05 1.09 1.13 1.17 1.2 1.23 1.26 1.29 1.32 1.34
ZMSM (RM) 0.1 0.03 −0.03 −0.1 −0.17 −0.24 −0.31 −0.38 −0.45 −0.52

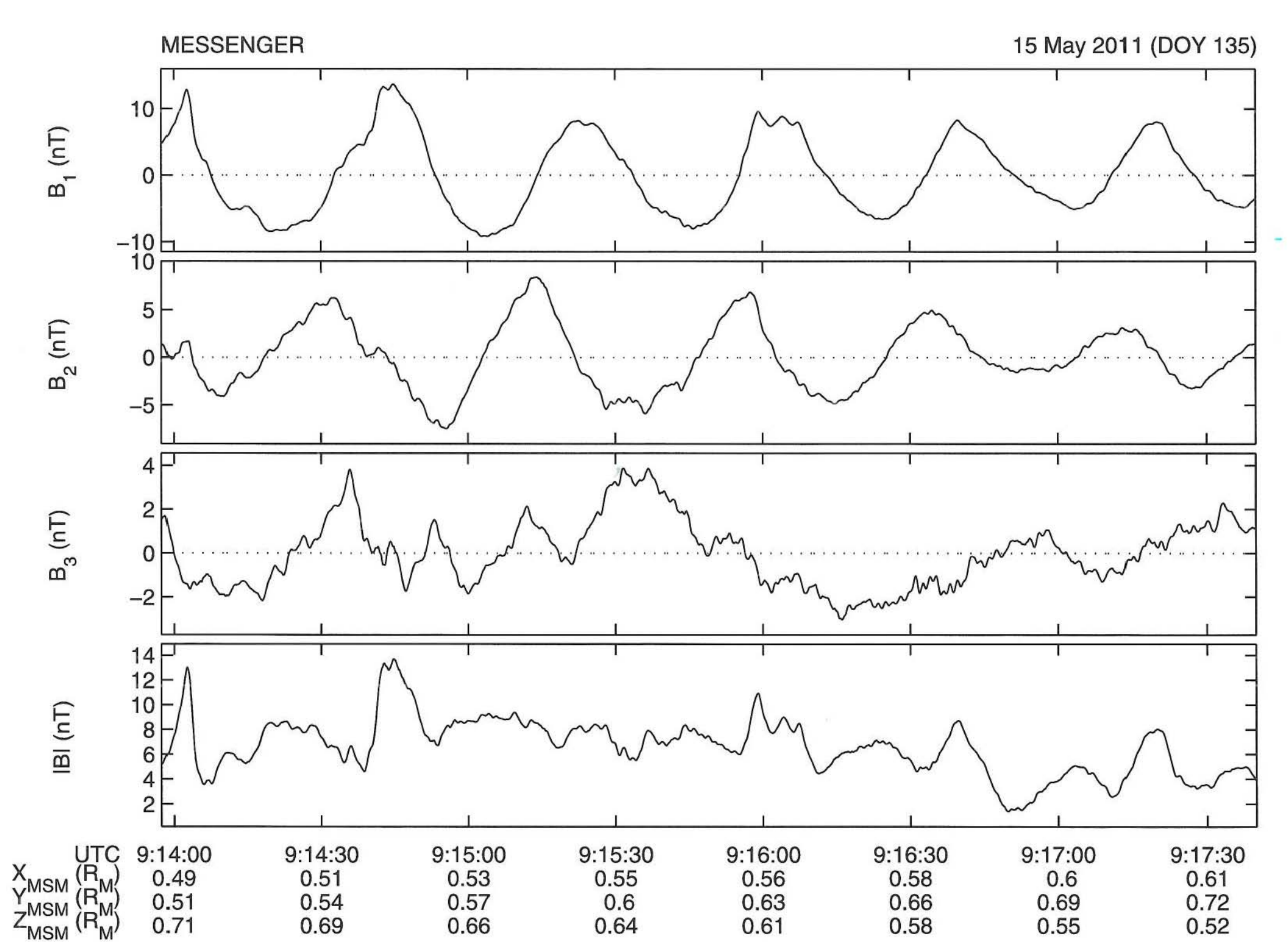
MESSENGER
15 May 2011 (DOY 135)
B1 (nT)
B2 (nT)
B3 (nT)
|B| (nT)
UTC 9:14:00 9:14:30 9:15:00 9:15:30 9:16:00 9:16:30 9:17:00 9:17:30
XMSM (RM) 0.49 0.51 0.53 0.55 0.56 0.58 0.6 0.61
YMSM (RM) 0.51 0.54 0.57 0.6 0.63 0.66 0.69 0.72
ZMSM (RM) 0.71 0.69 0.66 0.64 0.61 0.58 0.55 0.52

15 May 2011 (DOY 135) 09:14:00–09:17:40

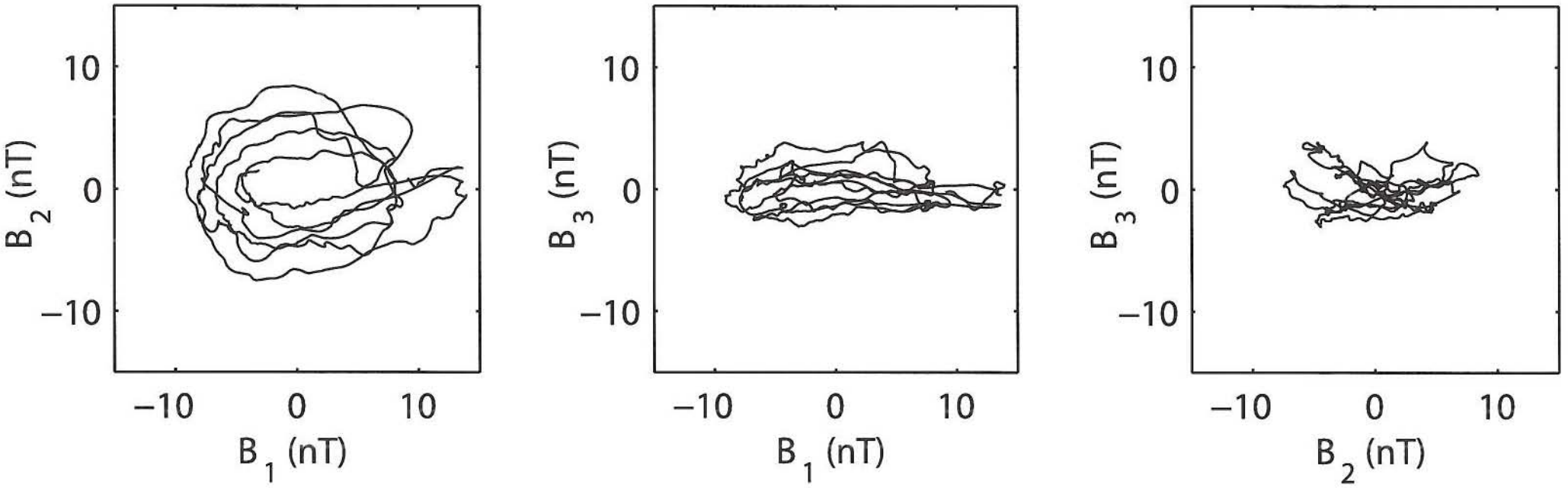

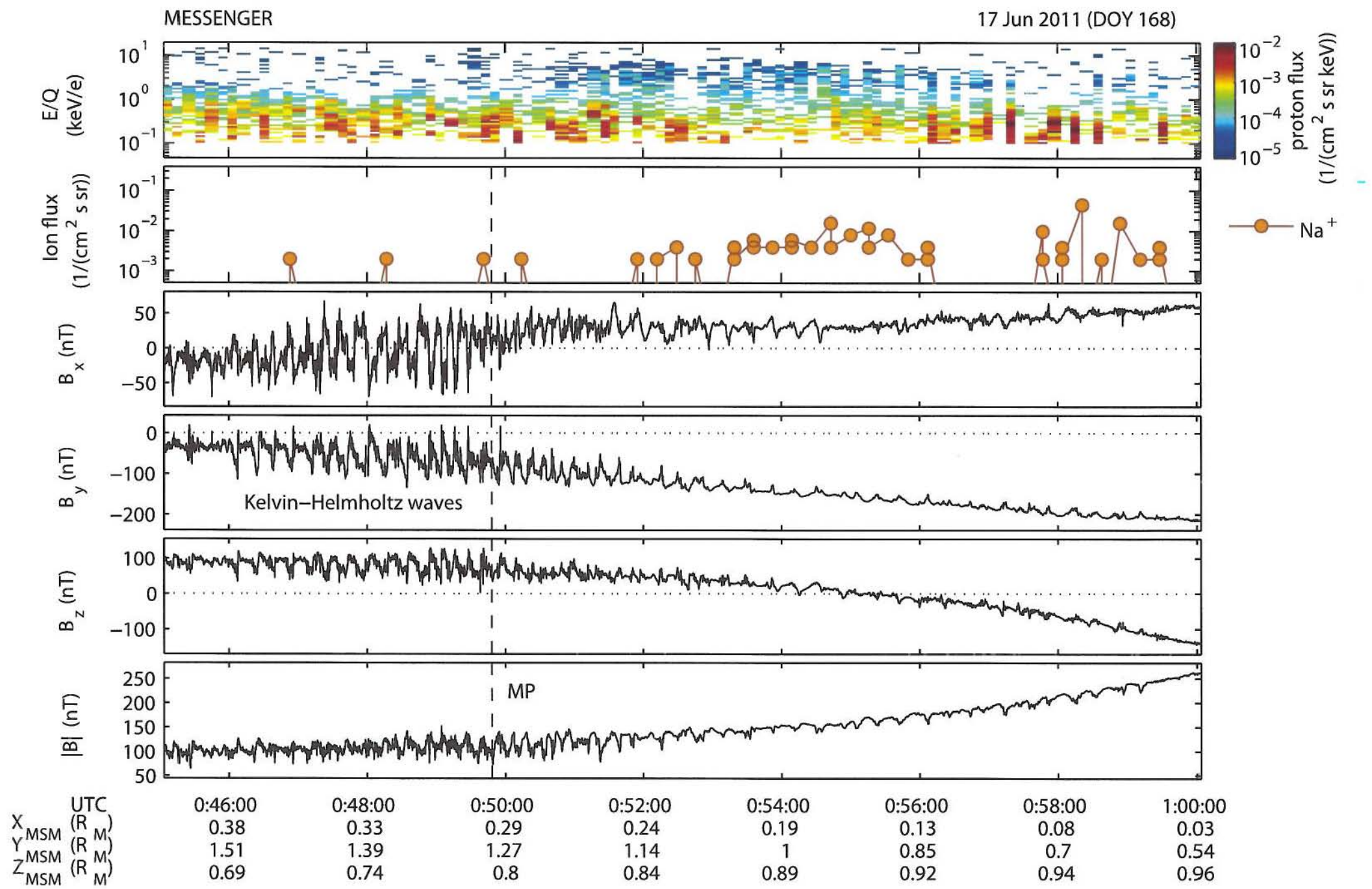
MESSENGER
17 Jun 2011 (DOY 168)
E/Q (keV/e)
proton flux (1/(cm^2 s sr keV))
Ion flux (1/(cm^2 s sr))
Na$^+$
B$_x$ (nT)
B$_y$ (nT)
Kelvin–Helmholtz waves
B$_z$ (nT)
|B| (nT)
MP
UTC
0:46:00 0:48:00 0:50:00 0:52:00 0:54:00 0:56:00 0:58:00 1:00:00
X$_{MSM}$ (R_M) 0.38 0.33 0.29 0.24 0.19 0.13 0.08 0.03
Y$_{MSM}$ (R_M) 1.51 1.39 1.27 1.14 1 0.85 0.7 0.54
Z$_{MSM}$ (R_M) 0.69 0.74 0.8 0.84 0.89 0.92 0.94 0.96

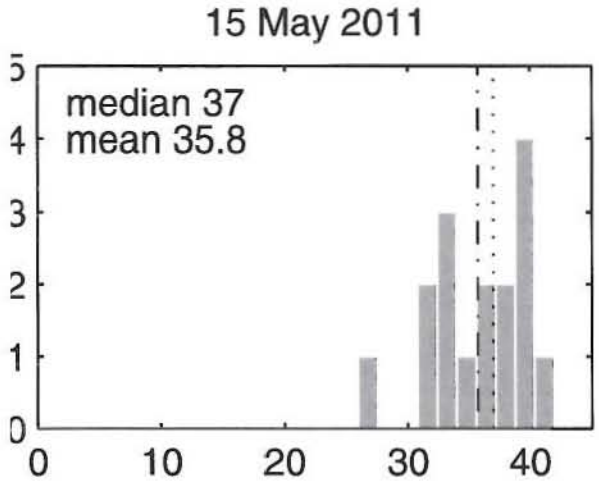
15 May 2011
median 37
mean 35.8
0
1
2
3
4
5
0
10
20
30
40

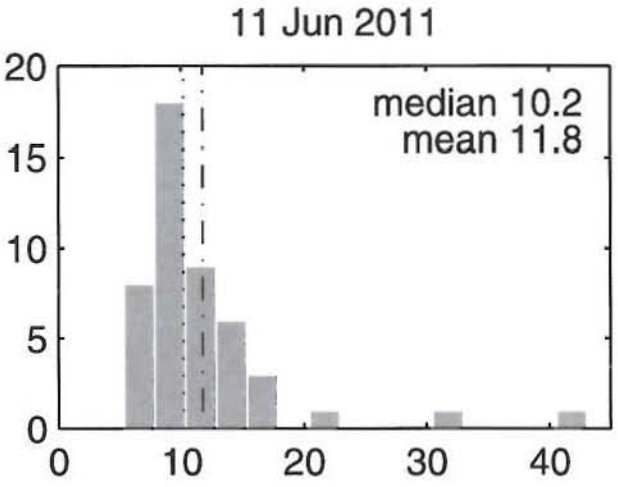
11 Jun 2011
median 10.2
mean 11.8
0
5
10
15
20
0
10
20
30
40

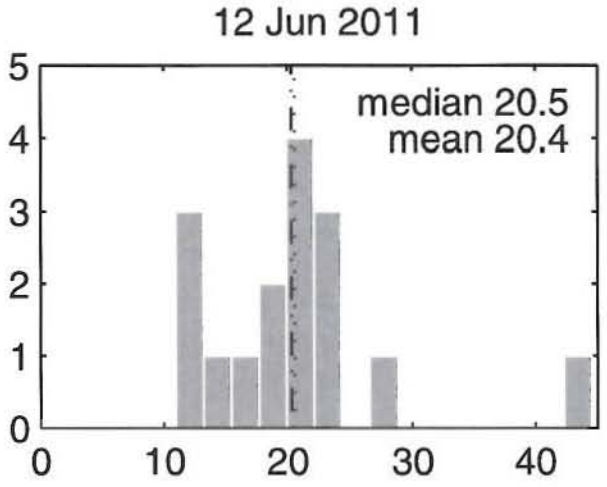
12 Jun 2011
median 20.5
mean 20.4
0
1
2
3
4
5
0
10
20
30
40

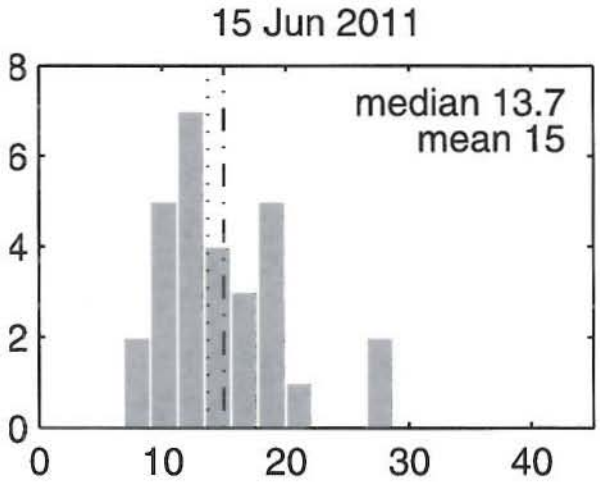
15 Jun 2011
median 13.7
mean 15
0
2
4
6
8
0
10
20
30
40

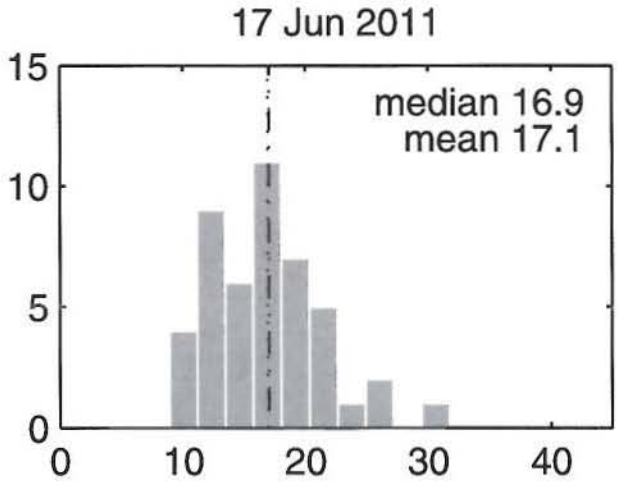
17 Jun 2011
median 16.9
mean 17.1
0
5
10
15
0
10
20
30
40

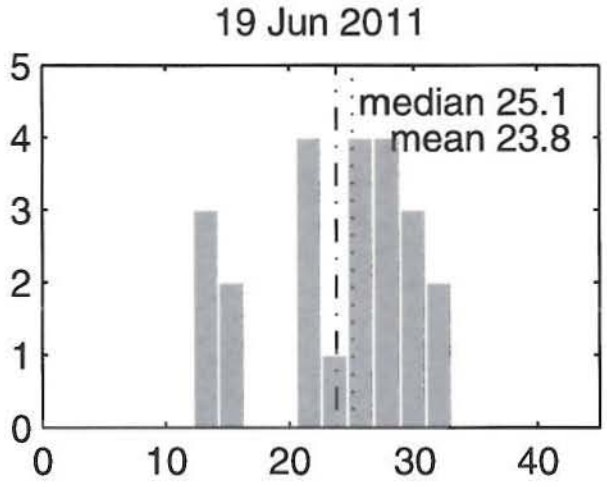
19 Jun 2011
median 25.1
mean 23.8
0
1
2
3
4
5
0
10
20
30
40